Enhanced Methane Production in Anaerobic Membrane Bioreactors: The Role of In-Situ Electro-Stimulation

Olga El Kik, Marc Heran, François Lestremau, Andrés Sauvêtre, François Zaviska, Geoffroy Lesage

Enhanced Methane Production in Anaerobic Membrane Bioreactors: The Role of In-Situ Electro-Stimulation

Olga El Kik [a,b], Marc Heran [b], François Lestremau [a], Andrés Sauvêtre [a], François Zaviska [b], Geoffroy Lesage [b,*]

[a] *Hydrosciences Montpellier, Univ Montpellier, IMT Mines Ales, IRD, CNRS, Ales, France*
[b] *IEM, Univ Montpellier, CNRS, ENSCM, Montpellier, France*

HIGHLIGHTS

- eGAnMBR and GAnMBR achieved >95 % organic matter removal from municipal wastewater.
- eGAnMBR exhibited higher resilience with faster stabilization after loading changes.
- Electrochemical stimulation boosted methane yield and reduced liquid saturation.
- Dissolved methane losses remained low even under low-temperature operation.
- Biogas was highly methane-rich, requiring minimal upgrading for grid injection.

GRAPHICAL ABSTRACT

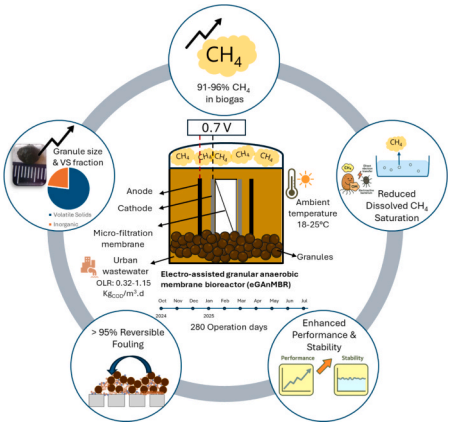

ABSTRACT

This study compared the 280-day performance of a granular anaerobic membrane bioreactor (GAnMBR) and its electro-assisted variant (eGAnMBR) treating domestic wastewater at ambient temperature across permeate fluxes of 1.7–5.9 L/m^2/h. Both systems achieved >95 % chemical oxygen demand removal. At moderate flux, eGAnMBR improved methane recovery by around 15 % versus the control and produced biogas up to 94 % methane. Lower effluent methane saturation suggested reduced dissolved-methane losses and lower greenhouse- gas risk. Despite slightly higher resistance from near-electrode cake, >95 % of fouling remained reversible; targeted design and operational optimization to limit cake and enhance local shear should support scale-up. Both systems remained net-energy-positive, with energy recovery above 0.76 kWh/m^3 at the highest loading and clearer eGAnMBR benefits at moderate loading and shorter hydraulic retention time. Overall, electro-stimulated GAnMBR improved methane valorization and process robustness while preserving a net-positive energy balance, indicating a practical path to scalable, low-carbon municipal treatment.

Keywords:
Bioelectrochemical granular reactor
Reversible cake fouling
Improved biogas recovery
Energy-positive operation
Low-strength wastewater

* Corresponding author.
E-mail address: geoffroy.lesage@umontpellier.fr (G. Lesage).

1. Introduction

Municipal wastewater is increasingly regarded as a renewable resource for water, energy, and nutrients within circular-economy strategies (Awasthi et al., 2023). This perspective prioritizes energy-positive treatment technologies that deliver high-quality effluent and resource recovery (Robles et al., 2021; Zhang and Liu, 2022).

In this context, anaerobic membrane bioreactors (AnMBRs) have emerged as an advanced solution that combines the benefits of anaerobic digestion with membrane separation, yielding reuse-quality effluent and enabling biomethane recovery (Anjum et al., 2021; Maaz et al., 2019). Despite their promise, AnMBRs still confront fouling, incomplete nutrient removal, dissolved-methane losses, large footprints from slow kinetics, and operational challenges with low-strength wastewater under ambient, fluctuating loads (Robles et al., 2021). These limitations are particularly pronounced in mainstream applications, where diluted municipal sewage and ambient operation contrast with sidestream or temperature-controlled setups. Overcoming these barriers remains essential to unlocking the full sustainability potential of AnMBRs for municipal and industrial wastewater treatment.

To address these limitations, granular sludge has gained attention for stabilizing and improving AnMBRs. Formed through interactions among diverse microorganisms, extracellular polymeric substances (EPS), and inorganic materials under selective conditions, granular sludge is characterized by its large particle size, compact structure, and superior settling ability (Show et al., 2020). Compared with floc sludge, granules offer higher microbial diversity and resilience to load fluctuations and toxic shocks (Gouveia et al., 2015). Integrated into AnMBRs (GAnMBRs), they can enhance organics removal and methane yield, and mitigate fouling (Deng et al., 2020; Sanchez et al., 2022a). Yet many high-flux studies relied on biogas sparging to control fouling, increasing energy use (0.04 to 1.56 kWh/m^3) (Gouveia et al., 2015; Lim et al., 2023; Wang et al., 2018). Operating GAnMBRs without sparging or other energy-intensive fouling control remains challenging but could improve net energy recovery (Sanchez et al., 2022a).

In parallel, the integration of bioelectrochemical systems (BES) with AnMBRs has emerged as a promising hybrid strategy that pairs electrode-driven stimulation with membrane separation, increasing resource recovery and producing high-quality effluent. In these configurations, electrodes stimulate electroactive consortia, enhancing organics degradation and methane production while limiting fouling via electrostatic effects and biofilm control (El Kik et al., 2024). Reported systems achieved >90 % chemical oxygen demand (COD) removal, higher methane yields, and up to 77 % longer fouling cycles than conventional AnMBRs (D. Hu et al., 2022; Zhao et al., 2021). These improvements have been attributed to reduced formation of EPS and soluble microbial products (SMP) under applied electric fields, which help maintain low transmembrane pressure (TMP) during extended operation (El Kik et al., 2021; Karimi et al., 2021). However, practical application still requires optimization of electrode configuration, energy input, and long-term operational stability to ensure that the additional electrical demand does not negate the energy gains associated with enhanced methane recovery (Han et al., 2023; Yang et al., 2018).

Beyond generic AnMBR-BES coupling, integrating BES with anaerobic granular sludge leverages granule architecture and electroactive niches for added gains. Reported systems achieved 86.8–100 % COD removal and up to 43 % higher methane yields, with methane content >80 % in some cases (Madondo et al., 2021; Zhao et al., 2019). Mechanistically, benefits arise from improved direct interspecies electron transfer (DIET) between exoelectrogenic and methanogenic populations, often facilitated by conductive materials (e.g., magnetite) or optimized electrodes (Wang et al., 2017; Zhao et al., 2019), and from electrochemical H_2 generation. In-situ H_2 supplies electron donors to hydrogenotrophic methanogens, enabling biological methanation that redirects pathways toward higher CH_4 and improves stability and efficiency under variable conditions (see Eqs. S1-S5 in Supplementary Material). While most demonstrations remain at the laboratory scale, the results underscore the potential of combining anaerobic granular sludge with BES to improve treatment efficiency, biogas recovery, and system resilience.

Building on this, coupling bioelectrochemical stimulation with anaerobic granular sludge within a membrane bioreactor configuration could combine the operational stability of granules, the electrochemical enhancement of microbial activity, and the high effluent quality of membrane separation. To date, only one study has explored electro-assisted filtration in the presence of granular sludge, showing that the applied electric field can promote sludge agglomeration and preserve granule integrity, thereby reducing membrane fouling (Wang et al., 2023). However, that work targeted a synthetic high-strength methanolic wastewater at 38 °C, used pre-adapted sludge fed with methanol only, and relied on continuous biogas recirculation (5 L/min) for mixing and fouling control. In response, the present study assessed this configuration under conditions representative of municipal treatment: ambient temperature, no energy-intensive gas sparging or forced recirculation, and a complex synthetic feed reproducing domestic organic fractions (Layer et al., 2019). Treatment performance, process stability, methane production, and overall energy balance were systematically evaluated and compared with a parallel GAnMBR, providing new insights into the feasibility and sustainability of coupling anaerobic granular sludge with electrochemical stimulation in membrane-based configurations.

2. Materials and methods

2.1. Reactor configuration and experimental setup

The experimental setup consisted of two identical GAnMBRs, one conventional and one electro-assisted (eGAnMBR). Both reactors were equipped with flat-sheet Kubota ultrafiltration membranes (Japan; pore size 0.4 μm, effective area 0.11 m^2) operated at constant flux by a permeate pump. The feed pump was regulated by a liquid level controller, while the supernatant was continuously withdrawn from the top and recirculated to the bottom at 5.55 L/h using a peristaltic pump (Watson Marlow®, 520S, UK). In the eGAnMBR, the membrane module was positioned between two nickel mesh cathodes (335 × 255 mm, 2 mm thick; 20 × 10 mm mesh), with Grade-2 titanium anodes (335 × 255 × 2 mm) overlaid with graphite sheets placed in the bulk at around 10 mm from the cathodes; both electrode types were procured from Ampere Industrie (France). A schematic of the eGAnMBR configuration is shown in Fig. 1, while additional details of the membrane-electrode assembly and the underlying electro-microbial interactions are provided in Fig. S1 in the Supplementary Material. The eGAnMBR was operated at a constant applied voltage of 0.7 V, previously reported to enhance microbial activity (El Kik et al., 2024).

2.2. Reactor startup and operation

The lab-scale GAnMBR and eGAnMBR were inoculated with acclimated anaerobic granular sludge from a previous study (Sanchez et al., 2022a) at initial concentrations of 86.33 ± 6.59 g TS/L and fed with a synthetic medium representative of low-strength domestic wastewater (Layer et al., 2019). The feed primarily contained soluble substrates, with sodium acetate as the main carbon source, supplemented by sodium propionate, glucose, small amounts of starch, peptone, and amino acids. Phosphate buffer and $NaHCO_3$ were added to provide phosphorus and alkalinity. The detailed composition (g/L) is provided in Table S1 of the Supplementary Material. Feed solutions were prepared weekly, stored at 4 °C under continuous stirring, and characterized by an average soluble COD (sCOD) of 485 ± 98 mg/L, particulate COD of 25 ± 2.5 mg/L, and dissolved organic carbon (DOC) of 162 ± 32 mg/L. The reactors were operated for 280 days (1 October 2024 to 7 July 2025), with the influent flow increasing progressively, thereby increasing the

organic load. Table 1 presents the operational conditions across the four periods of the experiment. The data shown are for the eGAnMBR; the GAnMBR followed similar trends with slight differences.

2.3. Monitoring and analytical methods

Performance monitoring focused on COD removal, biogas production, and TMP, while detailed organic matter (OM) characterization was conducted to elucidate interactions with the membrane and granules.

2.3.1. Characterization of dissolved organic matter by COD, DOC, and 3DEEM

COD was measured twice weekly in feed, supernatant, and permeate samples using LCK 314 or LCK 414 test kits (Hach, Germany) and quantified with a UV–Vis spectrophotometer (DR3900, Hach, Germany). For removal calculations, samples were pre-filtered through 0.22 μm syringe filters to determine sCOD, which was used as the performance indicator given the largely soluble influent. Complementary total COD measurements were performed during method validation to confirm that total and soluble fractions exhibited consistent removal trends. DOC was analyzed with a Shimadzu TOC-L analyzer equipped with an OCT-L autosampler. Three-dimensional excitation-emission matrix (3DEEM) fluorescence spectroscopy was performed weekly on supernatant and permeate samples pre-filtered at 1.2 μm (Grade GF/C, Whatman, UK), using a FL 6500 spectrofluorometer (PerkinElmer, USA). 3DEEM spectra contained Rayleigh and Raman scattering, which were corrected in MATLAB® by subtracting the pure water matrix (Zepp et al., 2004), before analyzing major fluorophore groups (Jacquin et al., 2017). Then, the integrated 3DEEM signal (A.U./nm^2) were grouped into three regions: regions I + II (Ex 200–250 nm, Em 280–380 nm) for protein-like substances, regions III + V (Ex 200–250/250–500 nm, Em 380–600 nm) for humic-like substances, and region IV (Ex 250–340 nm, Em 280–380 nm) for SMP-like substances.

2.3.2. TMP, granules, and electrochemical monitoring

Pressure sensors (ATM.ECO, Sensor Technik Sirnach, Switzerland) were installed to record atmospheric, headspace, and permeate pressures every 30 min, allowing accurate calculation of TMP. In addition to continuous TMP monitoring, membrane fouling was assessed during cleaning events using the resistance-in-series method, enabling the identification of different scales of fouling and their reversibility (Sanchez et al., 2022b). To assess biomass structure, granules were periodically sampled and characterized for their mineral and organic fractions according to Standard Methods. At the end of the operational period, granule particle size distribution (PSD) was assessed by wet sieving with mesh sizes of 1.0 mm, 0.630 mm, and 0.125 mm, allowing classification into four categories: large granules (>1 mm), medium (0.630–1 mm), small (0.125–0.630 mm), and fines or flocculent material (<0.125 mm). An external power supply (model AL 924A, ELC, France) provided a constant voltage to the circuit, while a high-resolution PicoLog data logger recorded the voltage drop across a fixed external resistor (10 Ω) connected in series with the eGAnMBR electrodes. The current was then calculated using Ohm's law.

Table 1
Operational conditions over the four experimental periods for the eGAnMBR system.

Timeline (d)	Days 1–140	Days 141–197	Days 211–244 & 268–281	Days 198–210 & 253–267
Duration (d)	140	57	48	28
HRT (h)	32.56 ± 2.40	19.06 ± 2.87	16.81 ± 0.96	9.56 ± 1.44
OLR ($kg_{COD}/m^3/d$)	0.32 ± 0.11	0.65 ± 0.22	0.74 ± 0.16	1.12 ± 0.29
Jw (LMH)	1.69 ± 0.14	2.98 ± 0.52	3.62 ± 0.17	5.88 ± 0.85
T (°C)	18.67 ± 1.68	20.20 ± 1.21	25.49 ± 1.43	23.54 ± 0.97

Abbreviations: HRT = hydraulic retention time (h); OLR = organic loading rate (kgCOD/m^3/d); Jw = water flux (L/m^2/h); T = temperature (°C).

2.3.3. Biogas composition and methane production

Gaseous methane production was continuously monitored using volumetric gas meters (MilliGas Counter®, Ritter, Germany). Production was normalized to standard conditions based on daily average temperature and pressure. Biogas composition (N_2, CH_4, CO_2) was analyzed by gas chromatography (Clarus 400, PerkinElmer, USA) equipped with a thermal conductivity detector. Dissolved methane was quantified using the headspace equilibration method (Sanchez et al., 2022a) based on the ideal gas law, partial pressures, and Henry's law equilibrium. Dissolved methane was monitored approximately every

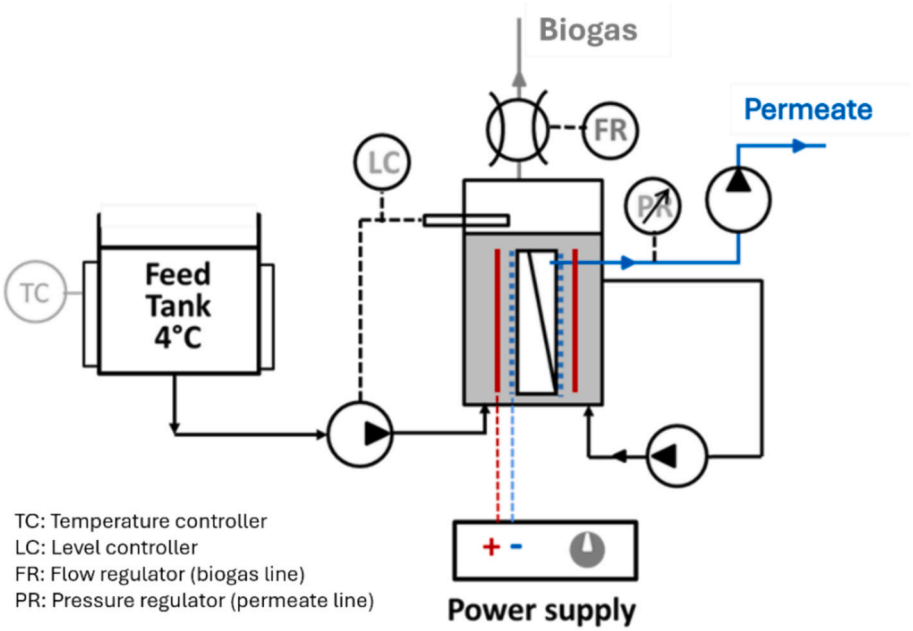

Fig. 1. Schematic of the electro-assisted granular anaerobic membrane bioreactor (eGAnMBR) operated with granular sludge under a 0.7 V DC electric field.

two weeks throughout the 280-day operation to capture temporal variations. Then, total methane yield (NL-CH_4/g$COD_{removed}$) was calculated by combining gaseous and dissolved fractions normalized by net COD removal ($COD_{Influent} - COD_{Effluent}$). Period-level average methane yields were computed as the ratio of cumulative methane produced to the cumulative net COD removed over each operational period (i.e., ratio of sums), which limits bias from day-to-day variability or missing measurements and provides a representative mean under steady operation. The methane saturation degree was further calculated to assess the extent of dissolved methane accumulation in the effluent. The theoretical dissolved methane concentration was estimated from the methane mole fraction measured in the reactor headspace according to Henry's law (Eq. (1)) and compared with the experimentally measured concentration. The methane saturation degree was then expressed as the ratio between the measured and the theoretical concentrations (Eq. (2)):

$$C_{CH4}^{effluent^*} = \frac{H^*}{P_T y_{CH4}} \times MM(CH_4) \quad (1)$$

$$Saturation degree = \frac{C_{CH4}^{effluent}}{C_{CH4}^{effluent^*}} \quad (2)$$

where $C_{CH4}^{effluent^*}$ is the theoretical dissolved methane concentration in the effluent (mg/L), P_T the biogas pressure (atm), y_{CH4} the methane mole fraction in the biogas, H* Henry's constant (mol/L.atm), $MM(CH_4)$ the molar mass of methane (g/mol), and $C_{CH4}^{effluent}$ the measured dissolved methane concentration in the effluent (mg/L).

2.3.4. COD partitioning and mass balance

A complete COD mass balance (gCOD/d) was performed according to Eq. (3):

$$Q_L COD_{in} - 0.67 Q_L SO4_{in} = Q_L COD_{out} + Q_L COD_{membrane} + Q_G COD_{CH4}^G + Q_L COD_{CH4}^L + V\frac{\Delta COD_{Biomass}}{\Delta t} \quad (3)$$

where a fraction of the influent COD was subtracted to account for oxidation by sulfate-reducing bacteria, using an empirical factor of 0.67 g COD per g SO_4^{2-} reduced. COD_{in} and COD_{out} represent the daily influent and permeate COD loads, calculated from measured concentrations (g_{COD}/L). $COD_{membrane}$ corresponds to the COD retained or accumulated on the membrane surface and in the fouling layer. COD_{CH4}^G and COD_{CH4}^L correspond to the COD methane equivalents of methane recovered in the gaseous and dissolved phases, respectively, with the daily loads obtained from the liquid (Q_L) and gas (Q_G) flow rates (L/d). The final term, $\Delta COD_{Biomass}/\Delta t$, represents the COD assimilated into microbial biomass, reflecting growth, renewal, and maintenance metabolism. Any remaining discrepancy in the COD balance (input minus quantified outputs) is reported as "Error + others" and reflects measurement uncertainty, sampling variability, and minor unaccounted sinks.

2.3.5. Energy Requirements and balance

The energy balance was assessed by comparing total electrical input (recirculation, permeate extraction, electrochemical supply) with the recoverable energy from biogas production. The energy consumed is given by Eq. (4):

$$Ee\,(kWh) = \left(\frac{\frac{Q1\rho gE1}{1000} + \frac{Q2\rho gE2}{1000}}{Q_2}\right) * V + \sum_1^n \left(IE_{ps}\Delta t - I^2 R_{ex}\Delta t\right) * \frac{1}{3600} \quad (4)$$

where Q_1 and Q_2 are the internal recycle and permeate flow rates (m^3/s); ρ_g is the unit weight of water (9800 N/m^3); E1 and E2 are the hydraulic head losses for circulation and transmembrane filtration (m); I is the measured current (A); E_{ps} the applied voltage (V); R_{ex} the external resistance (Ω); t is the integration time (s); and 1/3600 is the conversion factor from kJ to kWh.

The produced energy (E_{gas}) was estimated solely from methane production, as hydrogen was not detected or only at trace levels, being rapidly consumed via hydrogenotrophic pathways under the operating conditions:

$$E_{gas} = \rho_{Elec}\, n_{CH4}\, \Delta H_{CH4} \quad (5)$$

where nCH_4 is the number of methane moles derived from ideal gas law calculations, and ΔHCH_4 is its heat of combustion (891 kJ/mol). ρ_{Elec} is the conversion efficiency for the recovery of electrical energy from methane combustion (ρ_{Elec} = 33 % was applied reflecting typical values for microturbine or internal combustion engine systems).

3. Results and discussion

3.1. OM removal and biogas production

3.1.1. DOC and COD removal

Stable performance was maintained in both the GAnMBR and eGAnMBR throughout the 280-day operation, with more than 95 % organic matter removal and effluent COD consistently below the discharge limit of 125 mg/L despite increasing organic loading rate (OLR) (Fig. S2). On average, COD in the permeate was 55 % and 62 % lower than in the supernatant for GAnMBR and eGAnMBR, respectively, ensuring effluent quality through combined biological conversion and membrane separation. Only minor deviations occurred at startup, during disturbances, or during membrane cleaning, likely due to the removal of the fouling layer that had enhanced COD retention. Performance rapidly stabilized again, confirming the resilience of anaerobic granules and electro-assisted granular AnMBR.

3.1.2. Biogas production

Both the GAnMBR and eGAnMBR systems demonstrated stable and efficient methane production throughout the 280-day operation under the tested conditions. Methane percentage was largely unaffected by membrane fouling or organic loading, showing only a slight decline at the highest loads and remaining notably methane-rich in both systems (89–96 % CH_4, Fig. S3), well above the 50–70 % typically reported for anaerobic digestion. The eGAnMBR consistently achieved higher methane purity than the GAnMBR (94–96 % vs. 89–91 %, Table 4), underscoring its superior gas quality. As methane concentrations approached the 97 % threshold required for direct injection into the urban natural gas distribution grid, the need for conventional biogas upgrading processes could be substantially reduced.

However, high methane concentrations in biogas also increase the risk of losses through dissolution into the effluent. For this reason, the methane saturation degree, which reflects the balance between local methane production and the instantaneous degassing capacity, was investigated. The eGAnMBR consistently showed lower saturation levels than the control (0.716–0.747 vs. 2.574–1.896 in periods 1–2), suggesting that the applied electric field enhanced degassing through improved gas–liquid mass transfer as previously observed in microbial electrolysis systems (Keil et al., 2021; Lu et al., 2024). In parallel, bioelectrochemical stimulation is known to boost methanogenic activity by enriching electroactive microbial communities and facilitating DIET, further increasing methane production (Baek et al., 2021; Wang et al., 2022). These effects reduce greenhouse gas emissions and improve energy recovery.

During Period 3, both the OLR and the operating temperature increased (18.6–25.4 °C), decreasing methane solubility (Velasco et al., 2018) and enhancing gas–liquid transfer through increased turbulence (Sanchez et al., 2023), which together favored transfer to the gas phase. Under these conditions (periods 3 and 4), both systems approached

equilibrium (saturation < 1), resulting in minimal dissolved methane (<0.01 L/gCODremoved). As the eGAnMBR further generated more CH_4-rich biogas, the dissolved methane losses were slightly higher, implying that electrochemical assistance boosted methanogenesis more strongly than gas–liquid separation.

Regarding methane yield, the total yield including both biogas and dissolved methane (NL-CH_4/g$COD_{removed}$) was consistently higher in the eGAnMBR, reaching 0.323 ± 0.034 in Period 3, corresponding to 92 % of the theoretical maximum (0.35 NL-CH_4/g$COD_{removed}$), whereas the GAnMBR reached 0.293 ± 0.031 (84 %). This indicates enhanced conversion efficiency under electrochemical stimulation, likely due to improved methanogenic activity and more favorable electron transfer conditions. For operational yield, limited to the gaseous fraction and representing the actual recoverable energy of the system, values in Period 3 were 0.310 ± 0.033 and 0.275 ± 0.028 NL-CH_4/gCODremoved in the eGAnMBR and GAnMBR, respectively, corresponding to more than 95 % of the total yield.

3.1.3. *COD mass balance and biomass investigation*

The COD mass balance across the four operational periods is shown in Fig. 2. On average, the eGAnMBR converted about 10 % more influent COD into methane-equivalent COD than the GAnMBR, supporting enhanced methanogenic activity under electrochemical stimulation, although this advantage decreased slightly at the highest loading (Period 4). This aligns with previous electro-assisted anaerobic digestion studies reporting enhanced electron transfer and gas yields (Wang et al., 2024; Yu et al., 2021; Zhao et al., 2022). Despite the low operating temperatures, which typically favor methane dissolution, the fraction of COD lost as dissolved methane in periods 1 and 2 remained lower (11–13 %) than values previously reported for comparable systems (Sanchez et al., 2023, 2022a). As temperature and OLR increased in periods 3 and 4, this fraction decreased by >35 % in the GAnMBR and >25 % in the eGAnMBR, reaching about 7 % dissolved-methane losses. A carbon mass balance (Fig. S4) corroborates these trends, with CH_4 as the dominant gaseous carbon sink and CO_2 predominantly in the liquid phase.

The COD fraction attributed to microbial biomass in the reactor, encompassing growth, renewal, and maintenance, was estimated using an observed yield consistent with comparable anaerobic conditions (0.11–0.13 gVSS/g$COD_{removed}$) (Chen et al., 2017; Pacheco-Ruiz et al., 2021). The mass-balance error ("Error + others") was lower in the eGAnMBR than in the GAnMBR. This difference likely originates from a partial underestimation of methane production in the GAnMBR, as part of the biogas can remain entrapped within granular sludge or the fouling layer, leading to an incomplete recovery of both the gaseous and dissolved methane fractions. Such underestimation has been reported in previous AnMBR studies and is often linked to oversaturation of methane in the liquid phase under conditions of limited mixing and poor gas–liquid mass transfer (Robles et al., 2022). In contrast, electrochemical stimulation in the eGAnMBR enhanced liquid circulation and turbulence through localized electro-convective effects and bubble formation at the electrodes, which facilitated gas disengagement from the granules and improved overall methane release and measurement accuracy. This mechanism is consistent with the lower effluent methane saturation and faster headspace stabilization observed in the eGAnMBR.

3.2. *Dissolved organic matter, fouling behavior, and granules*

3.2.1. *Three-dimensional fluorescence excitation-emission matrix (3DEEM)*

To assess membrane selectivity and biological activity, 3DEEM fluorescence spectroscopy was applied to pre-filtration supernatants representing dissolved/colloidal organic matter (DCOM < 1.2 μm) and post-filtration permeates during stable operation. DCOM was expressed as the mean integrated 3DEEM volume across all tested organic loadings during stable operation (Fig. 3, Table 2), since no clear relationship between OLR and fluorescence intensity was observed, consistent with previous reports on low-OLR GAnMBRs (Vinardell et al., 2022). Supernatant and permeate spectra of both the GAnMBR and eGAnMBR exhibited two major fluorescence peaks: a protein-like region I + II (Ex/Em 220–230/320–350 nm), typically associated with tryptophan-containing compounds and soluble microbial products, and a humic-

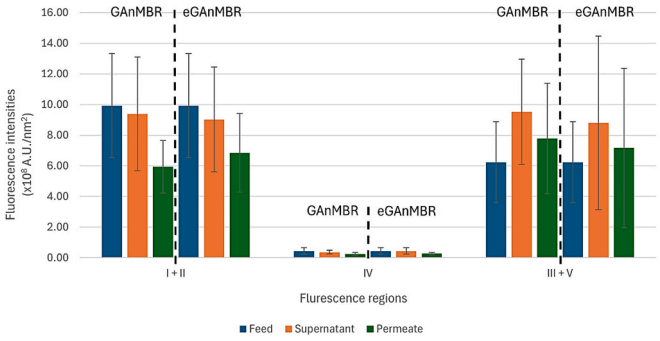

Fig. 3. Fluorescence intensities of organics in the GAnMBR and eGAnMBR reactors over a 120-day monitoring period, categorized for feed, supernatant, and permeate, and by fluorescence regions I + II (protein-like), IV (SMP-like), and III + V (humic-like).

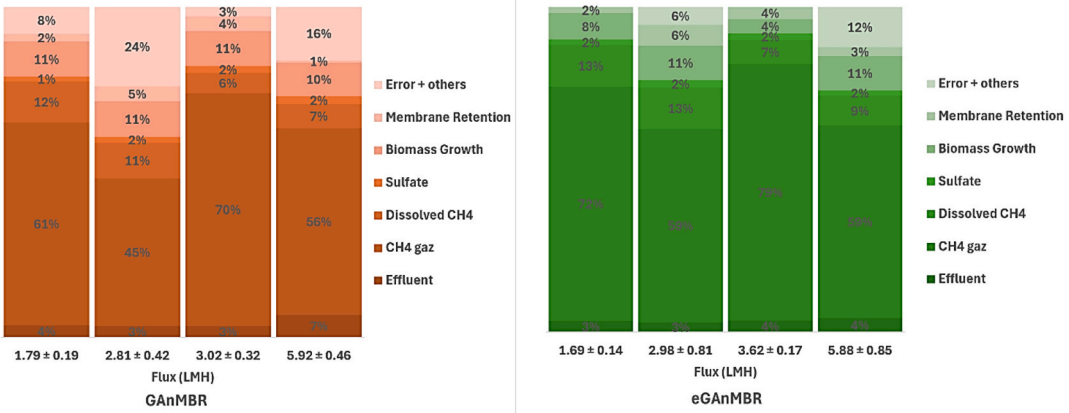

Fig. 2. Distribution of COD mass-balance partitions across four operational periods for GAnMBR (left) and eGAnMBR (right) at increasing flux. Stacked fractions show COD in the effluent, CH_4 (gas), dissolved CH_4 (liquid), sulfate reduction, biomass growth, membrane retention, and error/others (unaccounted and measurement error). Flux values for each period are displayed below the bars.

Table 2
Fluorescence intensities of organic compounds in the feed, supernatant, and permeate of GAnMBR and eGAnMBR systems, categorized by fluorescence regions I + II (protein-like), IV (SMP-like), and III + V (humic-like). The membrane retention percentage was calculated for each region. Data represent average values over the 120-day fluorescence monitoring period and are expressed as mean ± standard deviation, reflecting variations across different sampling times.

3DEEM Region	Feed ($\times 10^8$ A.U./nm^2)	System	Supernatant $\times$ 10^8 A.U./nm^2	Permeate $\times 10^8$ A.U./nm^2	Membrane Retention %
I + IIprotein like	9.94 ± 3.39	eGAnMBR	9.02 ± 3.41	6.84 ± 2.57	26.76 ± 12.18
		GAnMBR	9.39 ± 3.70	5.93 ± 1.72	33.92 ± 15.32
IVSMP	0.44 ± 0.21	eGAnMBR	0.44 ± 0.21	0.28 ± 0.07	36.18 ± 17.52
		GAnMBR	0.36 ± 0.12	0.25 ± 0.11	35.38 ± 12.73
III + Vhumic-like	6.24 ± 2.64	eGAnMBR	8.81 ± 5.66	7.17 ± 5.20	22.13 ± 16.53
		GAnMBR	9.53 ± 3.44	7.78 ± 3.60	18.71 ± 14.99
Total	16.70 ± 3.51	eGAnMBR	18.27 ± 7.04	14.29 ± 5.95	22.68 ± 10.11
		GAnMBR	19.29 ± 5.62	± 4.27	26.41 ± 12.15

like region III + IV (Ex/Em 250–270/400–450 nm), indicative of fulvic and humic acid-like substances commonly found in anaerobic effluents. Quantitatively, protein-like substances showed higher retention (27–34 %) than humic-like fractions (19–22 %) in both reactors.

The retention patterns observed are consistent with previous investigations: using a 0.3 μm PVDF microfiltration membrane (Vinardell et al., 2022) and a 0.04 μm PES ultrafiltration membrane (Sanchez et al., 2022a), comparable protein-like and humic-like fluorescence removal was reported, with region III + V identified as the least retained. This recurring observation across different membrane types and configurations suggests that the compounds contributing to fluorescence in region III + V, often associated with low-molecular-weight humic substances or microbial metabolites, are more hydrophilic and have simpler structures, making them less susceptible to size exclusion or adsorption on membrane surfaces. Their partial passage through the membrane may also reflect weaker interactions with the cake layer or biofilm components (Castilla-Rodriguez and Zhou, 2023). Comparison of permeate fluorescence before and after cleaning confirmed this trend: humic-like signals (region III + V) decreased by approximately 45 % in both reactors after cleaning, yet remained the least retained, showing that fouling did not enhance rejection. Overall, these results indicate that membrane retention mainly targets high-molecular-weight and hydrophobic DCOM fractions. Importantly, the applied current in the eGAnMBR did not alter the fate of dissolved or colloidal fractions compared with the GAnMBR. In both systems, the use of granular sludge minimized SMP-like fractions in the bulk phase, with region IV contributing less than 3 % of total fluorescence, consistent with the limited irreversible fouling observed in these reactors.

3.2.2. *Fouling behavior, membrane resistance and granule implications*

Membrane fouling behavior was assessed by monitoring the evolution of R_{total} over the 280-day operational period, supported by resistance partitioning after cleaning events and biomass characterization. As shown in Fig. 4, R_{total} steadily increased in both systems during each filtration period, with sharper increases after operational shifts to higher fluxes (Table 3). Under low-flux operation, the GAnMBR could be operated for more than 250 days without chemical cleaning. By contrast, at fluxes above 5 L/m^2/h (LMH), chemical cleaning was required approximately every 30 days. The eGAnMBR consistently exhibited higher membrane resistance than the GAnMBR, particularly during periods 3 and 4 when fluxes exceeded 5 LMH. This behavior was likely linked to the specific configuration of the eGAnMBR, in which the membrane is embedded between nickel mesh cathodes with only 0.8 mm spacing. Such a close arrangement may have created zones of reduced shear, promoting localized biomass deposition and cake accumulation. Notably, during the final operational phase, fouling behavior in the eGAnMBR improved following membrane maintenance and

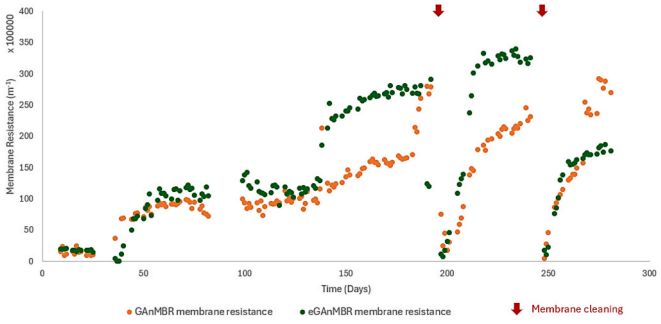

Fig. 4. Evolution of membrane resistance over time in GAnMBR (orange) and eGAnMBR (green) systems during 280 days of operation. Resistance trends are shown across four operational phases, with red arrows indicating membrane cleaning events. The eGAnMBR exhibited higher overall resistance, particularly during high-flux periods, though fouling remained fully reversible in both systems.

deliberate repositioning of the granules away from the membrane module. This adjustment likely enhanced local hydrodynamics, leading to a more stable R_{total}.

Despite the higher total resistance measured in the eGAnMBR, the membrane fouling resistance distribution showed that fouling remained largely reversible in both systems (>95 %) during all operating periods. This confirms that most of the accumulated resistance originated from loosely attached biomass, highlighting the protective role of granular sludge in limiting irreversible pore fouling. Importantly, under the low applied currents tested here, electrochemical stimulation did not produce an additional antifouling effect beyond that already provided by the granules, indicating that fouling was primarily governed by module configuration and local hydrodynamics.

To gain deeper insight into granule dynamics under electrochemical

Table 3
Fouling rate (dR/dt) in GAnMBR and eGAnMBR across four operational periods.

Variable	Period 1	Period 2	Period 3	Period 4
OLR (kg$_{COD}$/m^3/d)	0.32 ± 0.11	0.65 ± 0.22	0.74 ± 0.16	1.12 ± 0.29
Jw (LMH)	1.69 ± 0.14	2.98 ± 0.52	3.62 ± 0.17	5.88 ± 0.85
dR/dt (10^5/m/d) GAnMBR	0.038	0.12	0.12	8.8
dR/dt (10^5/m/d) eGAnMBR	0.018	0.12	0.12	13.6

Abbreviations: OLR = organic loading rate (kgCOD/m^3/d); Jw = water flux (L/m^2/h).

stimulation, the evolution of volatile solids (VS%) in membrane-associated biomass was monitored throughout the operational period. As shown in Fig. 5, the eGAnMBR exhibited significantly higher VS% at all measured time points, reaching 77 % on day 194 and gradually decreasing to 61 % by day 281, while the GAnMBR remained relatively stable around 48–52 %. This consistently higher VS% suggests enhanced accumulation of organic-rich biomass on the membrane surface in the electro-assisted configuration, likely driven by intensified and more diversified biological processes under the applied electric field. At the end of the experiment, PSD analysis (Fig. 5) further supported these findings: 78 % of the granules in the eGAnMBR exceeded 1 mm in diameter, compared to 63 % in the GAnMBR, while the fraction of fine particles (<0.125 mm) was lower in the eGAnMBR (14 % vs. 22 %). This shift toward larger and more stable granules may reflect improved microbial aggregation and biofilm structuring, potentially enhanced by electroactive species and modifications in EPS composition induced by the electric field. The resulting granules showed higher VS%, consistent with a more metabolically active biomass. These structural and functional advantages strengthen granule integrity, reduce the risk of degranulation, and provide clear benefits for scale-up, where sustained biomass retention and process robustness are critical for the long-term operation of eGAnMBR systems.

Beyond boosting methanogenesis (Section 3.1.2), DIET likely contributed to these structural outcomes. Electrically conductive networks formed by electroactive species facilitate electron shuttling across microbial layers, strengthening syntrophic coupling and enabling denser, larger, and more cohesive granules with higher VS%. Improved intra-granular electron flow may also reduce diffusional limitations, promoting both structural consolidation and metabolic resilience. These structural effects are consistent with the predominance of reversible (cake layer) fouling despite higher apparent resistance and provide a mechanistic bridge to the literature trends. Recent studies have demonstrated that electrochemical stimulation in anaerobic granular systems can significantly accelerate granule growth, up to fivefold within a few weeks, while promoting the development of layered microbial structures and selective enrichment of methanogenic and exoelectrogenic communities (Liu et al., 2011; Zhao et al., 2019). Simultaneously, reductions of 31–38.5 % in membrane fouling rate and up to 77.4 % in attached-phase EPS concentrations have been reported, supporting a strong link between electrochemical operation, mitigation of SMPs, and biomass consolidation on granule surfaces (D. Hu et al., 2022). These combined effects support the development of a more concentrated and metabolically active biomass, while maintaining a fouling profile dominated by reversible surface deposition rather than irreversible internal pore blockage.

Although membrane resistance was generally higher in the eGAnMBR, system performance remained stable due to the predominantly reversible nature of fouling and the limited contribution of intrinsic membrane resistance. Resistance trends stabilized after the last cleaning and granule repositioning at higher flux, and more than 95 % of total resistance was reversible (Fig. 4), indicating configuration-driven cake rather than intrinsic pore blocking. These findings underscore the importance of reactor design in managing biomass distribution and minimizing surface accumulation. Accordingly, optimization should prioritize local hydrodynamics near narrowly spaced electrodes and module layout. In addition to enhancing localized shear, other strategies may further reduce cake layer formation, including optimizing granule-membrane spacing to limit direct contact, orienting membranes to favor cross-flow dynamics, implementing intermittent filtration or relaxation phases to facilitate biomass detachment, and applying periodic gas scouring to disrupt surface buildup. In practice, this includes increasing electrode-membrane spacing, using more open meshes or segmented cathodes set back from the membrane to reduce shadowed zones, and programming brief flush/relax cycles in addition to steady operation. Surface modifications of electrodes or membranes can also reduce microbial adhesion, while controlling sludge age and composition may help limit EPS and SMP production. Periodic redistribution of granules can prevent packing near the module, and low-voltage pulsed energization or brief polarity-reversal bursts can discourage cake consolidation while preserving DIET benefits.

3.3. Energy balance

The energy balance was assessed by comparing the total electrical input (power supply and pumping) with the recoverable energy from methane, assuming a 0.33 conversion efficiency from methane combustion to electricity. As detailed in Table 4, both systems maintained net-positive energy balances throughout the operation, with energy recovery consistently exceeding consumption under all tested conditions.

In Period 1, characterized by low OLR and long hydraulic retention time (HRT), energy recovery was modest due to limited methane production relative to electrical input. Net energy values were similar for both systems (0.164–0.169 kWh/m^3). The net-to-produced energy ratios were 78 % for GAnMBR and 67 % for eGAnMBR, with the latter lower, reflecting the extra power required by the electrochemical supply. In Period 2, with electricity consumption unchanged and OLR increased to 0.6–0.7 $kg_{COD}/m^3/d$, methane generation improved in both systems, yielding a higher net energy gain in the eGAnMBR (0.359 kWh/m^3) compared to the GAnMBR (0.265 kWh/m^3). In Period 3, operated under thermally favorable conditions (25 °C) and with a reduced HRT (around 17 h), the performance gap between systems was most pronounced: 0.555 kWh/m^3 in the eGAnMBR versus 0.444 kWh/m^3 in the GAnMBR.

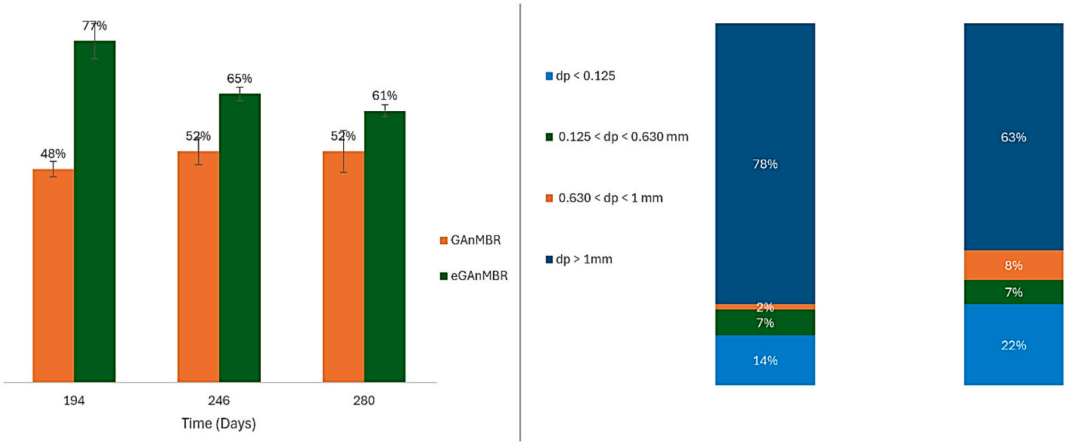

Fig. 5. (Left) Volatile suspended solids (%VS) in membrane-associated biomass measured at days 194, 246, and 280 in GAnMBR and eGAnMBR systems. (Right) Particle size distribution of granules on day 280, categorized by diameter ranges for both systems.

Table 4
Biogas and net energy performance of eGAnMBR and GAnMBR systems over four periods.

Parameter	eGAnMBR	GAnMBR	eGAnMBR	GAnMBR	eGAnMBR	GAnMBR	eGAnMBR	GAnMBR
Periods	**Period 1**		**Period 2**		**Period 3**		**Period 4**	
Time(Days)	D1-D140		D141-D197		D211-D247 / D268-D280		D198-D210 / D253-D267	
Flux ($L/m^2/h$)	1.69 ± 0.14	1.79 ± 0.19	2.98 ± 0.52	2.81 ± 0.42	3.62 ± 0.17	3.02 ± 0.32	5.88 ± 0.85	5.92 ± 0.46
Temperature(°C)	18.67 ± 1.68	18.56 ± 1.61	20.20 ± 1.21	19.98 ± 1.26	25.49 ± 1.43	25.42 ± 1.40	23.54 ± 0.97	23.52 ± 0.89
Hydraulic Retention Time(h)	32.56 ± 2.40	31.27 ± 3.01	19.06 ± 2.87	19.94 ± 4.01	16.81 ± 0.96	18.28 ± 1.73	9.56 ± 1.44	9.27 ± 0.72
Organic Loading Rate ($KgCOD/m^3/d$)	0.32 ± 0.11	0.33 ± 0.11	0.65 ± 0.22	0.61 ± 0.12	0.74 ± 0.16	0.61 ± 0.17	1.12 ± 0.29	1.15 ± 0.24
CH_4 percentage in biogas (%)	94	89	96	89	91	91	91	91
CH_4 rate(mL/d)	478.80	463.81	862.58	599.97	1253.63	953.35	1618.34	1573.69
Saturation degree	0.716 ± 0.227	2.574 ± 0.625	0.747 ± 0.221	1.896 ± 0.493	0.346 ± 0.125	0.691 ± 0.028	0.798 ± 0.000	0.778 ± 0.000
Gaseous methane Yield (NL/$gCOD_{removed}$)	0.254 ± 0.071	0.209 ± 0.053	0.254 ± 0.035	0.182 ± 0.044	0.310 ± 0.033	0.275 ± 0.028	0.281 ± 0.051	0.258 ± 0.043
Dissolved methane yield (NL/$gCOD_{removed}$)	0.046 ± 0.016	0.045 ± 0.016	0.057 ± 0.012	0.048 ± 0.010	0.013 ± 0.007	0.004 ± 0.007	0.001 ± 0.000	0.001 ± 0.000
Total methane yield ($NL/gCOD_{removed}$)	0.299 ± 0.073	0.254 ± 0.055	0.311 ± 0.037	0.231 ± 0.045	0.323 ± 0.034	0.279 ± 0.029	0.282 ± 0.051	0.258 ± 0.043
Positive energy balance (kWh/m^3)	0.169	0.164	0.359	0.265	0.555	0.442	0.795	0.763

In Period 4, corresponding to the shortest HRT (around 9 h) and highest OLR (1.1–1.2 $kg_{COD}/m^3/d$), both systems reached their highest absolute recoveries, with the eGAnMBR maintaining a slight advantage (0.795 vs 0.763 kWh/m^3).

To provide plant-scale perspective, Period 4′s high-flux operation was used for an order-of-magnitude extrapolation. As noted in Section 3.2.2, chemical cleanings at this flux occur about every 30 days (12 per year), totaling 360 events over 30 years. Cumulative chlorine exposure was conservatively capped at half of a published hollow-fiber threshold (reported at 500,000 mg/L/h; Robles et al., 2014); membrane life is therefore unlikely to be limited by chemical exposure over this horizon, and replacement is not assumed in this scenario. Using the EU sizing proxy for large wastewater treatment plants (≥100,000 population equivalents (PE), 0.2 m^3/PE/d), the reference influent is 20,000 m^3/d. At Period 4 flux, the required membrane area is around 138,890 m^2; at 50 €/m^2 this corresponds to 6.9 M€ in membrane purchase cost. With a methane yield of 0.28 $NL/gCOD_{removed}$ and 33 % electrical efficiency, the 30-year, 5 %-discounted present value of electricity revenue is about 8.8 M€, which by itself offsets the membrane purchase cost. A full techno-economic assessment is needed to resolve site-specific trade-offs and identify an operating window that maintains elevated flux and OLR without intensive cleaning, thereby supporting robust economics and durable operation.

4. Conclusion

This work demonstrated that both GAnMBR and eGAnMBR systems effectively treated low-strength domestic wastewater at ambient temperature achieving over 95 % organic matter removal while maintaining energy-positive operation. The electro-assisted configuration not only enhanced methane yield and generated high-purity biogas (94–96 % CH_4) requiring minimal upgrading for grid injection, but also exhibited greater resilience, with faster stabilization following loading fluctuations. Thus, electrochemical stimulation further boosted methane production and reduced methane saturation in the liquid phase, contributing to improved environmental performance, process robustness and energy recovery efficiency. This was more noticeable under moderate organic loading and shortened HRT, where the gradual formation of larger, enriched granules reflected improved microbial aggregation. Although internal membrane fouling remained low in the eGAnMBR, total resistance increased due to cake buildup associated with narrow electrode spacing. Fouling was manageable at low permeate flux, while chemical cleaning was required about every 30 days for flows greater than 5 LMH. Despite this, more than 95 % of fouling was reversible in both systems, and the overall energy balance remained positive. Practically, optimizing layout, promoting cross-flow with brief relaxation or flush cycles, and applying low-voltage pulsed operation can sustain methanogenesis gains while limiting reversible cake growth.

CRediT authorship contribution statement

Olga El Kik: Writing – original draft, Visualization, Methodology, Investigation, Data curation. **Marc Heran:** Writing – review & editing, Validation, Supervision, Conceptualization. **François Lestremau:** Writing – review & editing, Supervision, Project administration, Funding acquisition. **Andrés Sauvêtre:** Writing – review & editing, Supervision. **François Zaviska:** Writing – review & editing, Methodology. **Geoffroy Lesage:** Writing – review & editing, Validation, Supervision, Project administration, Methodology, Investigation, Funding acquisition, Conceptualization.

Declaration of competing interest

The authors declare that they have no known competing financial interests or personal relationships that could have appeared to influence the work reported in this paper.

Appendix A. Supplementary data

Supplementary data to this article can be found online at https://doi.org/10.1016/j.biortech.2025.133720.

Data availability

Data will be made available on request.

References

Anjum, F., Khan, I.M., Kim, J., Aslam, M., Blandin, G., Heran, M., Lesage, G., 2021. Trends and progress in AnMBR for domestic wastewater treatment and their impacts on process efficiency and membrane fouling. Environ. Technol. Innov. 21, 101204. https://doi.org/10.1016/j.eti.2020.101204.

Awasthi, M.K., Ganeshan, P., Gohil, N., Kumar, V., Singh, V., Rajendran, K., Harirchi, S., Solanki, M.K., Sindhu, R., Binod, P., Zhang, Z., Taherzadeh, M.J., 2023. Advanced approaches for resource recovery from wastewater and activated sludge: a review. Bioresour. Technol. 384, 129250. https://doi.org/10.1016/j.biortech.2023.129250.

Baek, G., Saikaly, P.E., Logan, B.E., 2021. Addition of a carbon fiber brush improves anaerobic digestion compared to external voltage application. Water Res. 188, 116575. https://doi.org/10.1016/j.watres.2020.116575.

Castilla-Rodriguez, E., Zhou, H., 2023. Organic compounds responsible for the fouling of ultrafiltration membrane treating algae-laden water. Membranes (basel) 13. https://doi.org/10.3390/membranes13090787.

Chen, R., Nie, Y., Ji, J., Utashiro, T., Li, Q., Komori, D., Li, Y.-Y., 2017. Submerged anaerobic membrane bioreactor (SAnMBR) performance on sewage treatment: removal efficiencies, biogas production and membrane fouling. Water Sci. Technol. 76, 1308–1317. https://doi.org/10.2166/wst.2017.240.

Deng, L., Guo, W., Ngo, H.H., Zhang, J., Liang, S., 2020. 5 - Advanced anaerobic membrane bioreactors: Performance enhancers and their hybrid systems. In: Ngo, H. H., Guo, W., Ng, H.Y., Mannina, G., Pandey, A. (Eds.), Current Developments in Biotechnology and Bioengineering. Elsevier, pp. 109–142. https://doi.org/10.1016/B978-0-12-819852-0.00005-1.

El Kik, O., Issa, L., Katuri, K.P., Saikaly, P.E., Alameddine, I., El-Fadel, M., 2021. Coupling anaerobic fluidized membrane bioreactors with microbial electrolysis cells towards improved wastewater reuse and energy recovery. J. Environ. Chem. Eng. 9, 105974. https://doi.org/10.1016/j.jece.2021.105974.

El Kik, O., Lesage, G., Zaviska, F., Sauvêtre, A., Heran, M., Lestremau, F., 2024. Synergistic approach for enhanced wastewater treatment: Harnessing the potential of bioelectrochemical systems in integration with anaerobic membrane bioreactors. J. Environ. Chem. Eng. 12, 113162. https://doi.org/10.1016/j.jece.2024.113162.

Gouveia, J., Plaza, F., Garralon, G., Fdz-Polanco, F., Peña, M., 2015. A novel configuration for an anaerobic submerged membrane bioreactor (AnSMBR). long-term treatment of municipal wastewater under psychrophilic conditions. Bioresour. Technol. 198, 510–519. https://doi.org/10.1016/j.biortech.2015.09.039.

Han, Y., Cai, T., Yin, J., Li, W., Li, S., Qiu, B., Lu, X., Zhou, Y., Zhen, G., 2023. Impact of sandwich-type composite anodic membrane on membrane fouling and methane recovery from sewage sludge and food waste via electrochemical anaerobic membrane bioreactor. Bioresour. Technol. 382, 129222. https://doi.org/10.1016/j.biortech.2023.129222.

Jacquin, C., Lesage, G., Traber, J., Pronk, W., Heran, M., 2017. Three-dimensional excitation and emission matrix fluorescence (3DEEM) for quick and pseudo-quantitative determination of protein- and humic-like substances in full-scale membrane bioreactor (MBR). Water Res. 118, 82–92. https://doi.org/10.1016/j.watres.2017.04.009.

Karimi, L., Hazrati, H., Gharibian, S., Shokrkar, H., 2021. Investigation of various anode and cathode materials in electrochemical membrane bioreactors for mitigation of membrane fouling. J. Environ. Chem. Eng. 9, 104857. https://doi.org/10.1016/j.jece.2020.104857.

Keil, T.M., Windisch, D., Joukov, V., Niedermeier, J., Schulz, W., Albrecht, J., 2021. Enhanced performance of microbial electrolysis cells using microstructured electrodes. Materwiss Werksttech 52, 279–288. https://doi.org/10.1002/mawe.202000198.

Layer, M., Adler, A., Reynaert, E., Hernandez, A., Pagni, M., Morgenroth, E., Holliger, C., Derlon, N., 2019. Organic substrate diffusibility governs microbial community composition, nutrient removal performance and kinetics of granulation of aerobic granular sludge. Water Res. X 4, 100033. https://doi.org/10.1016/j.wroa.2019.100033.

Lim, Z.K., Liu, T., Zheng, M., Rattier, M., Keller, J., Yuan, Z., Guo, J., Hu, S., 2023. Membrane reciprocation as energy-efficient fouling control with high biogas recovery in a pilot-scale anaerobic membrane bioreactor. Resour. Conserv. Recycl. 190, 106849. https://doi.org/10.1016/j.resconrec.2022.106849.

Liu, Y., Zhang, Y., Quan, X., Chen, S., Zhao, H., 2011. Applying an electric field in a built-in zero valent iron – Anaerobic reactor for enhancement of sludge granulation. Water Res. 45, 1258–1266. https://doi.org/10.1016/j.watres.2010.10.002.

Lu, X., Yadav, D., Wang, J., Jing, L., Zhu, Y., Ma, L., Jing, D., 2024. Hydrogen bubble evolution and gas transport mechanism on a microelectrode determined by cathodic potential and temperature. Phys. Fluids 36. https://doi.org/10.1063/5.0213398.

Maaz, M., Yasin, M., Aslam, M., Kumar, G., Atabani, A.E., Idrees, M., Anjum, F., Jamil, F., Ahmad, R., Khan, A.L., Lesage, G., Heran, M., Kim, J., 2019. Anaerobic membrane bioreactors for wastewater treatment: Novel configurations, fouling control and energy considerations. Bioresour. Technol. 283, 358–372. https://doi.org/10.1016/j.biortech.2019.03.061.

Madondo, N.I., Tetteh, E.K., Rathilal, S., Bakare, B.F., 2021. Synergistic effect of magnetite and bioelectrochemical systems on anaerobic digestion. Bioengineering 8. https://doi.org/10.3390/bioengineering8120198.

Pacheco-Ruiz, S., Heaven, S., Banks, C.J., 2021. Operation of submerged anaerobic membrane bioreactors at 20 °C: effect of solids retention time on flux mixed liquor characteristics and performance. Processes 9. https://doi.org/10.3390/pr9091525.

Robles, Á., Jiménez-Benítez, A., Giménez, J.B., Durán, F., Ribes, J., Serralta, J., Ferrer, J., Rogalla, F., Seco, A., 2022. A semi-industrial scale AnMBR for municipal wastewater treatment at ambient temperature: performance of the biological process. Water Res. 215, 118249. https://doi.org/10.1016/j.watres.2022.118249.

Robles, A., Ruano, M.V., Ribes, J., Seco, A., Ferrer, J., 2014. Model-based automatic tuning of a filtration control system for submerged anaerobic membrane bioreactors (AnMBR). J. Memb. Sci. 465, 14–26. https://doi.org/10.1016/j.memsci.2014.04.012.

Robles, Á., Serralta, J., Martí, N., Ferrer, J., Seco, A., 2021. Anaerobic membrane bioreactors for resource recovery from municipal wastewater: a comprehensive review of recent advances. Environ. Sci. (camb) 7, 1944–1965. https://doi.org/10.1039/D1EW00217A.

Sanchez, L., Carrier, M., Cartier, J., Charmette, C., Heran, M., Steyer, J.-P., Lesage, G., 2022a. Enhanced organic degradation and biogas production of domestic wastewater at psychrophilic temperature through submerged granular anaerobic membrane bioreactor for energy-positive treatment. Bioresour. Technol. 353, 127145. https://doi.org/10.1016/j.biortech.2022.127145.

Sanchez, L., Lesage, G., Demiral, Y.O., Rodriguez-Roda, I., Heran, M., Blandin, G., 2022b. Revealing the role of supernatant and granular sludge fractions on granular anaerobic membrane bioreactor fouling. J. Water Process Eng. 49, 103168. https://doi.org/10.1016/j.jwpe.2022.103168.

Sanchez, L., Vinardell, S., Charreton, J., Heran, M., Lesage, G., 2023. Assessing the impact of granular anaerobic membrane bioreactor intensification on treatment performance, membrane fouling and economic balance. J. Environ. Chem. Eng. 11, 109369. https://doi.org/10.1016/j.jece.2023.109369.

Show, K.-Y., Yan, Y., Yao, H., Guo, H., Li, T., Show, D.-Y., Chang, J.-S., Lee, D.-J., 2020. Anaerobic granulation: a review of granulation hypotheses, bioreactor designs and emerging green applications. Bioresour. Technol. 300, 122751. https://doi.org/10.1016/j.biortech.2020.122751.

Velasco, P., Jegatheesan, V., Othman, M., 2018. Recovery of dissolved methane from anaerobic membrane bioreactor using degassing membrane contactors. Front. Environ. Sci. 6–2018.

Vinardell, S., Sanchez, L., Astals, S., Mata-Alvarez, J., Dosta, J., Heran, M., Lesage, G., 2022. Impact of permeate flux and gas sparging rate on membrane performance and process economics of granular anaerobic membrane bioreactors. Sci. Total Environ. 825, 153907. https://doi.org/10.1016/j.scitotenv.2022.153907.

Wang, D., Han, H., Han, Y., Li, K., Zhu, H., 2017. Enhanced treatment of Fischer-Tropsch (F-T) wastewater using the up-flow anaerobic sludge blanket coupled with bioelectrochemical system: effect of electric field. Bioresour. Technol. 232, 18–26. https://doi.org/10.1016/j.biortech.2017.02.010.

Wang, D., Hao, Z., Tao, S., Shi, Z., Liu, Z., Liu, E., Long, S., 2024. Enhanced methane production from waste activated sludge by microbial electrolysis cell assisted anaerobic digestion: Fate and effect of humic substances. Bioresour. Technol. 403, 130872. https://doi.org/10.1016/j.biortech.2024.130872.

Wang, K.M., Cingolani, D., Eusebi, A.L., Soares, A., Jefferson, B., McAdam, E.J., 2018. Identification of gas sparging regimes for granular anaerobic membrane bioreactor to enable energy neutral municipal wastewater treatment. J. Memb. Sci. 555, 125–133. https://doi.org/10.1016/j.memsci.2018.03.032.

Wang, X.-T., Zhang, Y.-F., Wang, B., Wang, S., Xing, X., Xu, X.-J., Liu, W.-Z., Ren, N.-Q., Lee, D.-J., Chen, C., 2022. Enhancement of methane production from waste activated sludge using hybrid microbial electrolysis cells-anaerobic digestion (MEC-AD) process – a review. Bioresour. Technol. 346, 126641. https://doi.org/10.1016/j.biortech.2021.126641.

Wang, Y., Gao, Y., Lu, X., Gadow, S.I., Zhuo, G., Hu, W., Song, Y., Zhen, G., 2023. Bioelectrochemical anaerobic membrane bioreactor enables high methane production from methanolic wastewater: roles of microbial ecology and microstructural integrity of anaerobic biomass. Chemosphere 339, 139676. https://doi.org/10.1016/j.chemosphere.2023.139676.

Yang, Y., Qiao, S., Jin, R., Zhou, J., Quan, X., 2018. Fouling control mechanisms in filtrating natural organic matters by electro-enhanced carbon nanotubes hollow fiber membranes. J. Memb. Sci. 553, 54–62. https://doi.org/10.1016/j.memsci.2018.02.012.

Yu, Z., Liu, W., Shi, Y., Wang, B., Huang, C., Liu, C., Wang, A., 2021. Microbial electrolysis enhanced bioconversion of waste sludge lysate for hydrogen production compared with anaerobic digestion. Sci. Total Environ. 767, 144344. https://doi.org/10.1016/j.scitotenv.2020.144344.

Zepp, R.G., Sheldon, W.M., Moran, M.A., 2004. Dissolved organic fluorophores in southeastern US coastal waters: correction method for eliminating Rayleigh and Raman scattering peaks in excitation–emission matrices. Mar. Chem. 89, 15–36. https://doi.org/10.1016/j.marchem.2004.02.006.

Zhang, X., Liu, Y., 2022. Resource recovery from municipal wastewater: a critical paradigm shift in the post era of activated sludge. Bioresour. Technol. 363, 127932. https://doi.org/10.1016/j.biortech.2022.127932.

Zhao, K., Su, F., Gu, K., Qi, J., Liu, R., Hu, C., 2021. Antifouling potential and microbial characterization of an electrochemical anaerobic membrane bioreactor utilizing membrane cathode and iron anode. Bioresour. Technol. 334, 125230. https://doi.org/10.1016/j.biortech.2021.125230.

Zhao, N., Treu, L., Angelidaki, I., Zhang, Y., 2019. Exoelectrogenic anaerobic granular sludge for simultaneous electricity generation and wastewater treatment. Environ. Sci. Technol. 53, 12130–12140. https://doi.org/10.1021/acs.est.9b03395.

Zhao, W., Su, X., Zhang, Y., Xia, D., Hou, S., Zhou, Y., Fu, H., Wang, L., Yin, X., 2022. Microbial electrolysis enhanced bioconversion of coal to methane compared with anaerobic digestion: Insights into differences in metabolic pathways. Energy Convers. Manag. 259, 115553. https://doi.org/10.1016/j.enconman.2022.115553.